ResearchGate

See discussions, stats, and author profiles for this publication at: https://www.researchgate.net/publication/258424801

Origin of Interfacial Nanoscopic Gaseous Domains and Formation of Dense Gas Layer at Hydrophobic Solid–Water Interface

ARTICLE *in* LANGMUIR · NOVEMBER 2013

Impact Factor: 4.46 · DOI: 10.1021/la403187p · Source: PubMed

CITATIONS
9

READS
31

3 AUTHORS, INCLUDING:

Hong Peng
University of Queensland
22 PUBLICATIONS **133** CITATIONS
SEE PROFILE

Greg R. Birkett
University of Queensland
31 PUBLICATIONS **212** CITATIONS
SEE PROFILE

Available from: Hong Peng
Retrieved on: 31 January 2016

Langmuir

Article

pubs.acs.org/Langmuir

Origin of Interfacial Nanoscopic Gaseous Domains and Formation of Dense Gas Layer at Hydrophobic Solid−Water Interface

Hong Peng, Greg R. Birkett, and Anh V. Nguyen*

School of Chemical Engineering, The University of Queensland, Brisbane, Queensland 4072, Australia

ABSTRACT: Interfacial gas enrichment (IGE) covering the entire area of hydrophobic solid−water interface has recently been detected by atomic force microscopy (AFM) and hypothesized to be responsible for the unexpected stability and anomalous contact angle of gaseous nanobubbles and the significant change from DLVO to non-DLVO forces. In this paper, we provide further proof of the existence of IGE in the form of a dense gas layer (DGL) by molecular dynamic simulation. Nitrogen gas adsorption at the water−graphite interface is investigated using molecular dynamic simulation at 300 K and 1 atm normal pressure. The results show that a DGL with a density equivalent to a gas at pressure of 500 atm is formed and equilibrated with a normal pressure of 1 atm. By varying the number of gas molecules in the system, we observe several types of dense gas domains: aggregates, cylindrical caps, and DGLs. Spherical cap gas domains form during the simulation but are unstable and always revert to another type of gas domain. Furthermore, the calculated surface potential of the DGL−water interface, −17.5 mV, is significantly closer to 0 than the surface potential, −65 mV, of normal gas bubble−water interface. This result supports our previously stated hypothesis that the change in surface potential causes the switch from repulsion to attraction for an AFM tip when the graphite surface is covered by an IGE layer. The change in surface potential comes from the structure change of water molecules at the DGL−water interface as compared with the normal gas−water interface. In addition, the contact angle of the cylindrical cap high density nitrogen gas domains is 141°. This contact angle is far greater than 85° observed for water on graphite at ambient conditions and much closer to the 150° contact angle observed for nanobubbles in experiments.

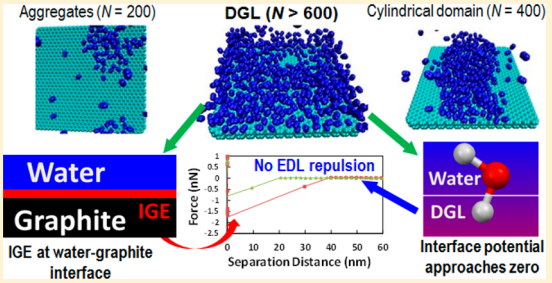

1. INTRODUCTION

Since their existence was first detected at the solid−water interface by atomic force microscopy (AFM) 20 years ago,[1] nanobubbles (or nanopancakes) have been produced via various formation procedures: solvent exchange,[2−4] substrate heating,[5,6] and electrical chemical formation[7,8] as imaged or detected by AFM[9−11] and recently by optical microscopy visualization.[12,13] Interfacial nanobubbles exhibit a number of peculiar properties compared to macro- or micro-sized bubbles, including unusually large contact angle values on the liquid side (about 150°) and longer lifetimes (hours to days) than expected.[10,11,14]

Several mechanisms have been proposed to fill the gap in understanding the experimental evidence: contamination layer model,[15] dynamic equilibrium model,[5,16,17] high density gas bubble model,[18,19] and recently contact line pinning model.[20,21] Seddon et al.[22] provided an extensive review on the contamination layer and dynamic equilibrium models. For the high density gas bubble and contact line pining models, it is hypothesized that very slow gas diffusion results in the long life of nanoscopic gas domains. However, none of these models can comprehensively explain the formation and stability of these nanoscopic domains.

Recently, Peng et al.[23] used the AFM force mapping technique and measured long-range attractive (nonDLVO) forces between an AFM tip and nannobubbles at the interface between water and highly ordered pyrolytic graphite (HOPG). One characteristic of the AFM characterization is the jump-in distance, i.e., where strong attraction force appears. The long-range attractive force over the surface is grouped into two areas: circular areas (nanobubbles) of long range forces with jump-in distances of approximately 30 nm and the area (assigned as non-nanobubbles) with smaller values of jump-in distance of approximately 15 nm. Both are outside the range of attraction from van der Waals forces which is expected at a distance of approximately 1−5 nm based on the DLVO theory.[24,25] The attraction between the tip and the surface after nanobubble generation is different from the attraction in the presence of repulsive force of the electrostatic double layer (EDL) interaction between the tip and the bare HOPG−water interface. Since attraction was detected over the whole surface by the force mapping technique, it was proposed that interfacial gas enrichment (IGE) layer covered the entire area with nanobubbles and would be responsible for the non-DLVO attractive forces. The lack of EDL repulsive interaction indicates that the surface potential of the water−IGE interface may be closer to 0 than that of normal gas bubble−water, at a value of −65 mV[26,27] (experimental data), and the potential of the HOPG−water interface at neutral pH, at −22 mV[28] (experimental data). From the AFM experiment series it was

Received: August 23, 2013
Revised: October 28, 2013
Published: November 8, 2013

 © 2013 American Chemical Society

hypothesized that the interface between the IGE and water was materially different from that of a regular water−gas interface. However, this mechanism is difficult to verify directly by experiments.

Molecular simulation has played an important role in understanding the formation of gas enrichment or nanobubbles on solid surfaces. Dammer and Lohse[17] performed molecular dynamics simulations of Lennard-Jones (LJ) gas−liquid mixtures to study the density profile of dissolved gas at hydrophilic and hydrophobic solid walls. They showed that there was significant gas enrichment near a hydrophobic wall. However, Bratko and Luzar[29] reported that the gas enrichment near the wall was not significant with varying interaction strengths when they used the simple point charge (SPC) model of water instead of LJ particles. Later, Sendner[30] also showed that different gases dissolved in water solution on a diamond-like structure solid surface. The gas enrichment for all gas types was modest and significant only within 1 nm of the surface. However, all these simulation works only reported the localized gas aggregates instead of a gas layer covering the surface.

Simulations of nanobubbles or multiple gas domains formed at solid surface are less numerous. Only Wang et al.[19] have reported the molecular simulation of nanobubbles or dense gas layers (referred to as micropancakes) at a water-graphite interface. They reported that the density of nanobubbles or micropancakes was much higher than gas at ambient conditions with values up to 40% of the saturated liquid at 77 K. Later, they proposed the high gas density theory to explain nanobubble stability based on gas diffusion theory.[18] However, their simulation only focused on formation of nanosized gas domains on the solid surface and did not explain the unusual large contact angle of nanosized gas domains.

Here, we utilize the molecular dynamics simulation to study nitrogen gas adsorption at the water−graphite interface. We first show that high density gas domains are stable and that these domains exist either as aggregates, cylinders, or gas layers, depending on the number of gas molecules in the system. The interfacial properties of the graphite−high density gas−water system, interfacial potential, and orientation of water molecules are used to explain why an AFM tip is repelled by a water−graphite interface but attracted to the gas−water interface of a gas layer on graphite. In addition, we show that the cylindrical high density gas domains have a contact angle comparable to those observed for nanobubbles in the AFM experiments. These will also assist in further understanding the formation and stability of multiple-type gas domains at the graphite−water interface.

2. MOLECULAR SIMULATION

2.1. Interaction Models. The SPC/E water model was used to describe the liquid water as this water model has been investigated comprehensively.[31−35] For nitrogen the universal force field (UFF) model[19] was used. The carbon parameters for solid graphite were the same as the values reported by Werder et al.[34] These potential parameters were also verified based on evaluating contact angle of water droplet on graphite described in section 2.3. Using this technique with a cylindrical drop, we calculated a contact angle of 85°, which agreed with the work of Werder et al.[34,35] The standard Lorentz−Berthelot type mixing rules were used to obtain the LJ parameters between atoms of different species. The sets of potential parameters used are shown in Table 1.

Table 1. Potential Parameters of Atoms Used in Simulation

atom	molecule	σ (nm)	ε (kJ/mol)	charge (e)
O	water	0.3166	0.6502	−0.8476
H	water	0	0	0.4238
N	nitrogen	0.3261	0.2887	0
C	graphite	0.3190	0.3920	0

2.2. Molecular Simulation Settings. The simulations were performed in the NVT ensemble (at constant particle number, volume and temperature) or NPT ensemble (at constant particle number, pressure and temperature) using the GROMACS package.[36] The temperature was fixed at 300 K by using Berendsen temperature coupling method. The system pressure was only applied to the normal to the solid surface and coupled by the Berendsen method at 1 atm. Both LJ and electrostatic interactions were truncated at 1.0 nm. Long-range electrostatic interactions were corrected by the Ewald summation method using particle mesh Ewald for the reciprocal part.[37] Two sheets of model graphite were placed at distance of 0.1 and 0.44 nm from bottom of simulation box with a surface area of 6.9 × 6.6 nm used to fit the periodicity of the graphite surface. The height of simulation box was varied based on the simulation conditions. The leapfrog method with a time step of 1 fs was used to integrate the particle motion. The running time ranged from 3 to 12 ns depending on the property of interest.

2.3. Contact Angle Simulation. We implemented the same procedure used in previous papers by our group[38,39] to obtain the contact angles, θ, for water droplets on the graphite surface and dense gas domains at the water−graphite interface. Here, we provide a brief description about this procedure. In general, the determination of contact angle by molecular simulation normally involves three steps. First, the ensemble average mass densities within grid volumes are calculated from the simulation relative to the center of mass of droplet. The grid points are then fitted with a spline to find the position of the interface at the defined interface density. Once the positions of the interface are obtained, the positions are fit with a circle function to calculate the contact angle.

The contact angle was calculated between the tangent to the curve (at contact point) of the fitting function and the solid surface. Here, we used mass center of the top layer of graphite (z = 0.44 nm) as the solid surface. Only grid volumes above the surface by a distance of at least 0.18 nm (z = 0.62 nm) were used in the fitting. For water droplets on the graphite surface, the position of the interface was defined as the being where the density was equal to half of the bulk water density (∼16.5 nm^{-3}). For dense gas domains between water and graphite, the position of interface was defined as the being where the density was equal to half of the equilibrium bulk density (∼4.5 nm^{-3}), as shown in Figure 1. In the following sections, we report the contact angle only from water side. So it is 180°−θ for dense gas domains and θ for water droplet.

2.4. Calculation of Interfacial Tensions for Liquid−Solid−Vapor Interfaces. We have used the weighted test-area method[38] to determine the interfacial tensions between liquid−vapor, solid−liquid, and solid−vapor phases in determining the Young's equation contact angle by Monte Carlo (MC) simulations. We have determined the interfacial tension for normal pressure nitrogen−graphite, normal pressure nitrogen−water, dense nitrogen−graphite, dense nitrogen−water, and water−graphite interfaces. The Steele potential was used to

dx.doi.org/10.1021/la403187p | Langmuir 2013, 29, 15266−15274

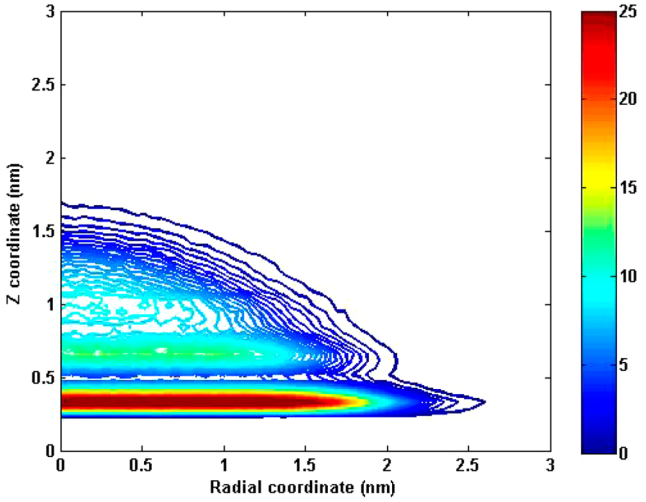

Figure 1. Density profile (in units of nm^{-3}) of nitrogen gas domain on top of graphite surface by molecular simulation. The z coordinates have been shifted to relate with solid surface at z = 0.44 nm. Note: water molecules are surrounded in this gas domain.

represent the graphite solid surface[40,41] for the surface tension calculations. For carbon, water, and nitrogen gas molecules, the parameters are same as in Table 1. Both LJ and electrostatic interactions were truncated at 1.2 nm without long-range corrections.[42]

2.5. Calculation of Interfacial Potential. The atomic approach was used to determine the effects of the atomic partial charge distributions on the electrostatic surface potential difference across the vapor−liquid interface. The surface potential difference across the interface is defined by[43,44]

$$\Delta\phi = \phi(z) - \phi(z_0) = \int_{z_0}^{z} E_z(z)\,\mathrm{d}z \tag{1}$$

Normally, z_0 is a reference point in the charge-free vapor region; $\phi(z)$ and $E_z(z)$ are the electrical potential and electric field derived from point charges along the z-axis across the vapor−liquid interface. $E_z(z)$ is calculated by integrating the charge distribution along the z-axis from the vapor to the liquid phase, i.e.

$$E_z(z) = \frac{1}{\varepsilon_0}\int_{z_0}^{z} \langle\rho_q(z)\rangle\,\mathrm{d}z \tag{2}$$

where ε_0 is the vacuum permittivity and $\langle\rho_q(z)\rangle$ is the ensemble averaged charge density profile which was evaluated in slabs of 0.05 nm thickness along the z-axis.

If we chose a value of 2.5 nm for z_0 for pure water system at 300 K, as shown in Figure 2, we obtain a surface potential difference value, $\Delta\phi$, of −600 ± 10 mV, which is close to the simulation values reported by other groups[32,43,45] but is significantly larger than the surface potential values from −40 to −65 mV reported from air-bubble experiments.[27,46,47] However, there is another electrical field zero point at z = 3.2 nm as a consequence of the reversal of electrical field which corresponds to the minimum value of the potentials. As studied by Wilson et al.,[44] this minimum value suggests that there are two different structural features of interfacial region between water and vapor, and this would represent the measured potential difference between interfacial and bulk water phases. We calculated the potential difference between minimum value and bulk water as −40 ± 10 mV. This value is much closer to the range of experimental zeta potential values. Here, we define this difference gap as the apparent interfacial potential.

$$\Delta\phi^{a} = \phi(z) - \phi(z_a) = \frac{1}{\varepsilon_0}\int_{z_a}^{z} E_z(z)\,\mathrm{d}z \tag{3}$$

where z_a = 3.2 nm is a reference point at which the electrical field change from positive to negative and $E_z(z_a)$ = 0. We use this value calculating the surface potential of systems in the following sections.

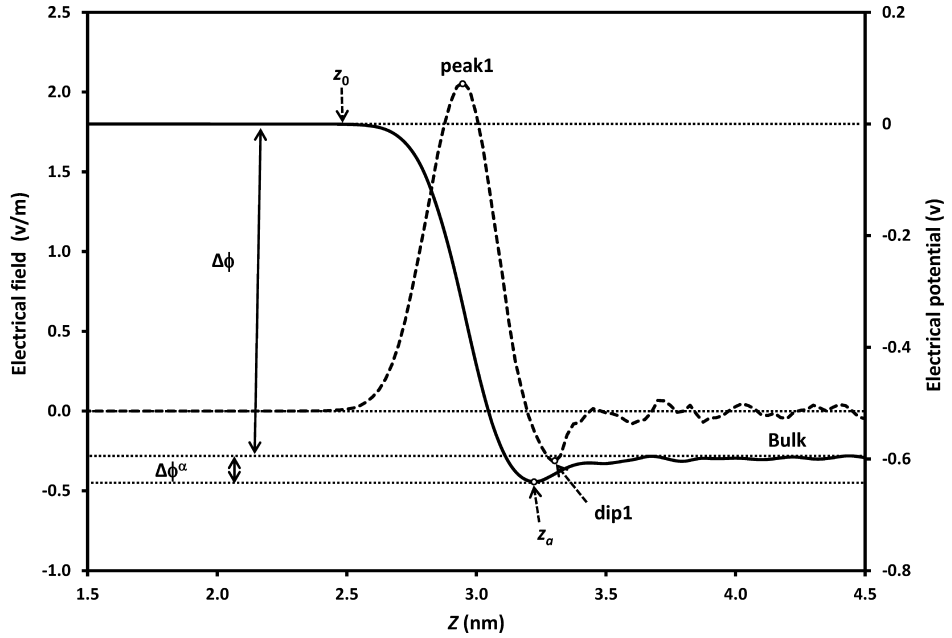

Figure 2. Electrical field (dashed line) and potential (solid line) as a function of distance across the vapor−water interface for pure water at 300 K. Dashed arrows at z_0 = 2.5 and z_a = 3.2 nm show the two places for calculating the potential differences. Peak 1 (point of maximum electrical field), dip1 (point of minimum electrical field), and bulk will be used for angle orientation.

dx.doi.org/10.1021/la403187p | *Langmuir* 2013, 29, 15266−15274

2.6. Local Density and Angle Orientation. As mentioned in the surface potential section, the structural analysis of water molecules at vapor−liquid interfaces, such as density and angle orientation, can be used to reveal changes of surface properties. To investigate the orientation of water molecules at vapor−liquid and solid−liquid interfaces, we recorded the two angles between water molecules and the interface normal (z-axis),[32,48] as shown in Figure 3. ϕ is the angle between the water dipole vector and the z-axis, and φ is the angle between an OH bond and the z-axis. The hydroxyl angle varies from 0° to 180° with angle of 90° corresponding to when the OH bond is parallel to the interface. The orientational distribution of water molecules is characterized by the distribution of the projection of the OH-bond vector to the surface normal, $P\{\cos(\varphi_i)\}$, which is calculated in the normal way as follows:

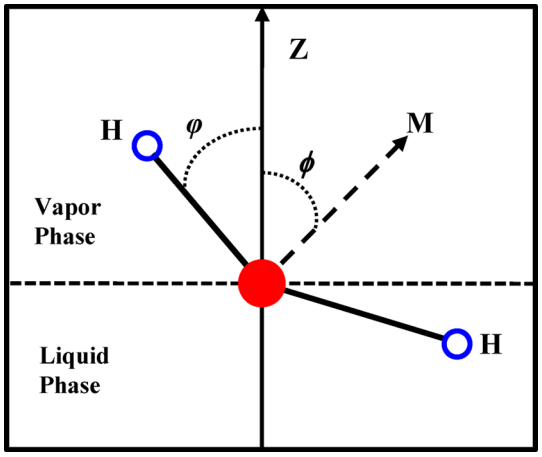

Figure 3. Schematic graph of the definition of the hydroxyl angle φ and dipolar angle ϕ for the water molecules. Two angles are defined with respect to the interface normal (z-axis).

$$P\{\cos(\varphi_i)\} = \frac{\langle \cos(\varphi_i) \rangle}{\sum_{i=1}^{n} \langle \cos(\varphi_i) \rangle} \quad (4)$$

where the angle brackets describe the arithmetical mean of the projections of the OH vectors in an interface slice (a sample bin), and n is the sampling number of cosine values of φ in the sampling bin. The simulation system is divided into 0.05 nm thick slices. Figure 4 shows the orientation profiles of water at the liquid−vapor interface for a system at 300 K. The water molecules show clearly double layer structures. At the outmost layer (peak 1) with thickness of 0.05 nm, one OH bond is pointing normal to the interface, and the other OH bond is forming an angle of 70° with the normal. At the innermost of interface (dip 1), the angle preference of OH bond is supplementary to the angle of OH bond from the peak 1 layer approximately. This phenomenon has also been reported by other researchers.[32,45]

3. RESULTS AND DISCUSSION

3.1. Multiple Types of Gas Domains Formed at Water−Graphite Interface. Besides nanobubbles, other types of gas domains (nanopancakes and gas layers) are reported using different methods of generating nanobubbles at the water−graphite interface.[23,49−51] In attempting to reproduce this variety in molecular simulation, we placed a varying number of nitrogen molecules (N = 100, 200, 300, 400, 600, 1000, and 2250) in a cubic grid on top of two layers of graphite. The initial nitrogen density in this grid is 8 nm^{-3}. The remainder of the simulation box, with dimensions of 6.9 × 6.6 × 7.0 nm, was filled with water molecules at a density of 33.1

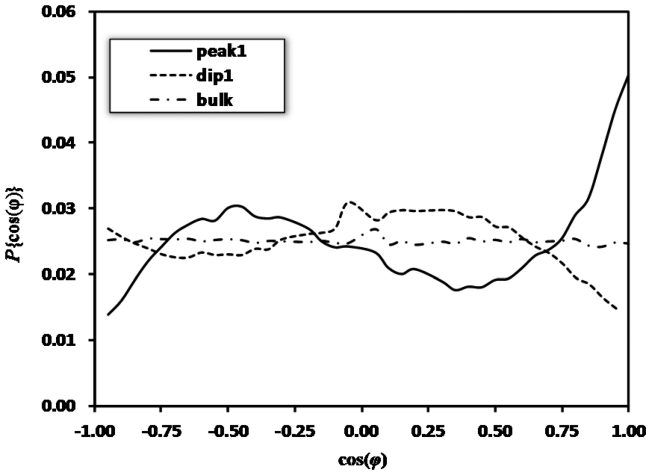

Figure 4. OH bond orientation of water molecules at vapor−liquid interface for one of OH bonds. Peak 1, dip 1, and bulk are defined in Figure 2.

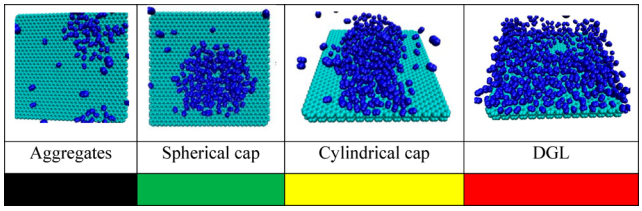

Figure 5. Color representation and snapshot from MD simulations for multiple gas domains on graphite surface (water molecules are omitted).

Table 2. Summary of Multiple Gas Domains Formed by Different Numbers of Gas Molecules and Running Time Used in the Simulation[a]

Number of N_2	Running Time (ns)						
	0.5	1	1.5	2.0	2.5	3.0	5.0
100							
200							
300							
400							
600							
1000							
2250							

[a]The color scheme for the domains is shown in Figure 5.

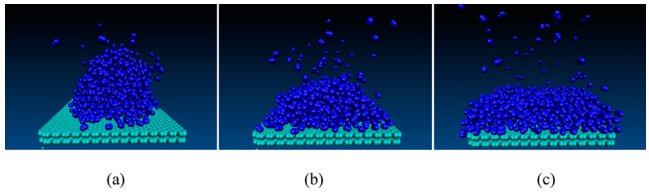

Figure 6. Snapshot of nitrogen gas domains formed during the molecular simulation with N = 1000 (a) at 0.5 ns, (b) at 1.5 ns, and (c) after 2.5 ns. Water molecules are not shown.

dx.doi.org/10.1021/la403187p | Langmuir 2013, 29, 15266−15274

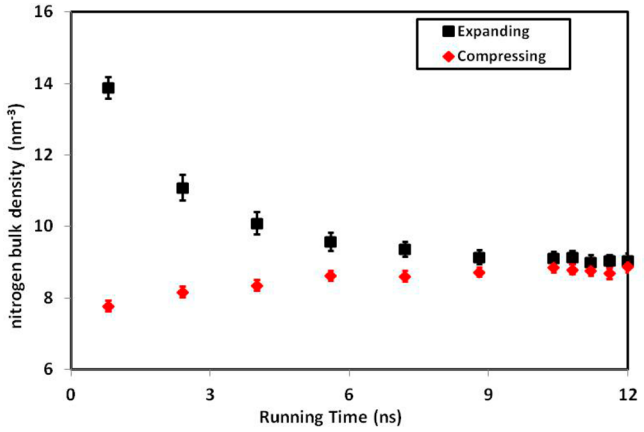

Figure 7. Density of the gas layer in the region between 2 and 3.5 nm from the surface versus running time in the expanding and compressing cases (refer to text).

nm^{-3}. The simulation is then run in the NPT ensemble at 300 K and 1 atm for over 5 ns.

As shown in Figure 5, depending on the number of gas particles used in the simulation, various nitrogen gas domains were formed: aggregates, spherical cap, cylindrical cap, and density gas layer (DGL).[60] For N = 100 and 200, the nitrogen gas molecules diffused into water and only formed some local aggregates. For N = 300 and 400, the nitrogen gas molecules formed only a cylindrical gas domain. For simulations with more than 600 nitrogen molecules, the nitrogen spread across the whole solid surface and formed a DGL. The density of DGL, 9.0 nm^{-3}, is about 50% of liquid nitrogen density (17.5 nm^{-3} or 806 kg/m^3) at 77 K.[52] This density is equivalent to a gas at 300 K and 500 atm. As shown in Table 2, we did not observe a stable spherical cap gas domain even though this domain was formed during the simulation time as shown in Figure 6.

Based on the density profiles shown in Figure 8, the calculated average number of nitrogen molecules for covering one layer of solid surface is approximately 164 (i.e., 6.6 nm × 6.9 nm × 0.4 nm × 9 nm^{-3}, where 0.4 nm is the distance between the first and second peaks). Combining with the data in Table 2, we see that when the number of gas molecules is insufficient for one layer, they tend to form local aggregates on

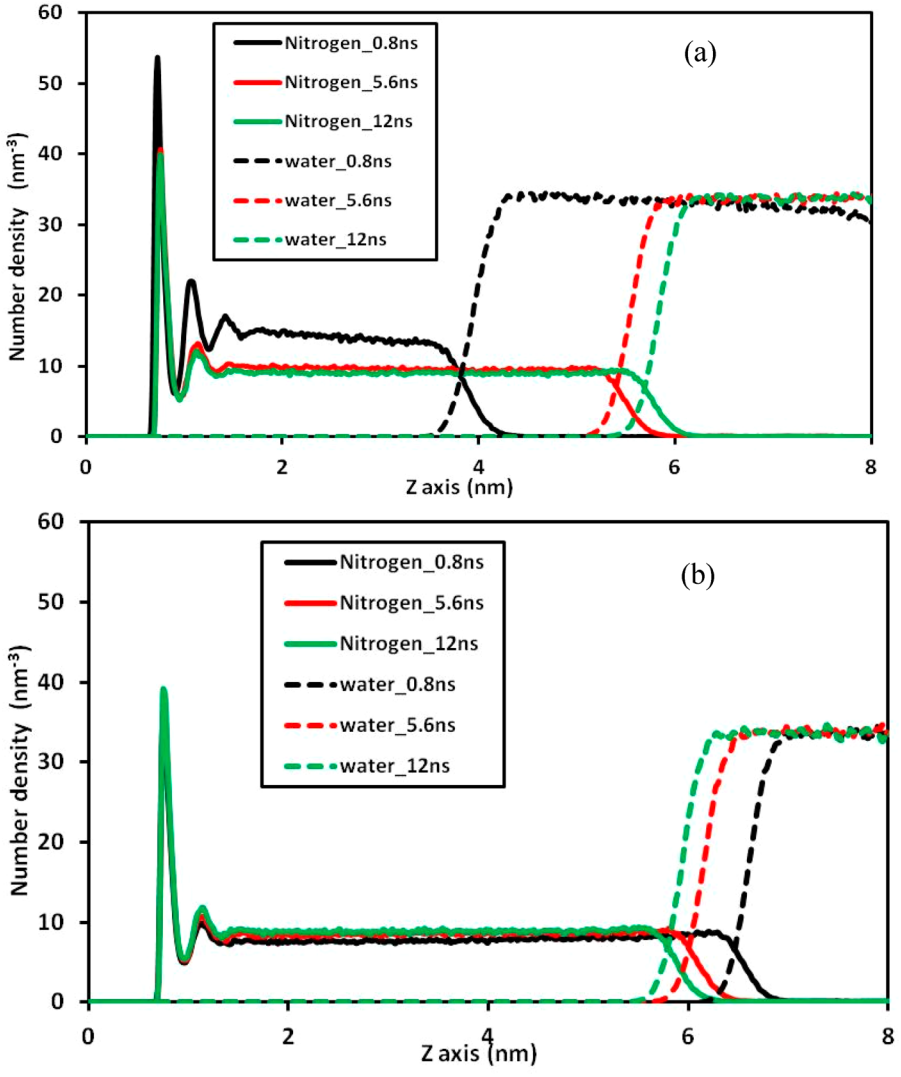

Figure 8. Nitrogen and water density profiles along the z-axis with three different running times for (a) the expanding case and (b) the compressing case.

dx.doi.org/10.1021/la403187p | *Langmuir* 2013, 29, 15266−15274

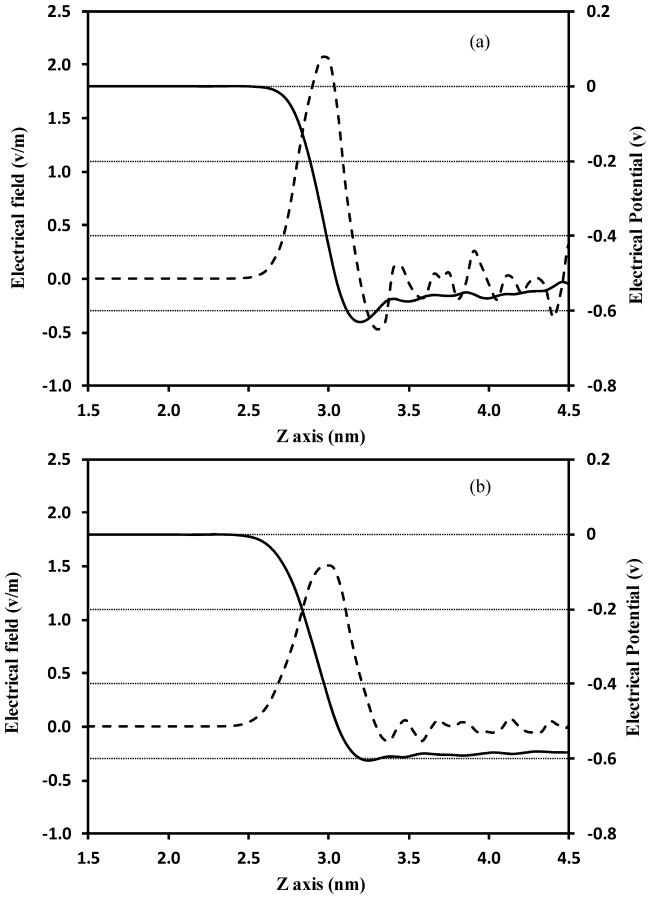

Figure 9. Electrical field and potential profiles of (a) the normal gas–water interface and (b) the DGL–water interface.

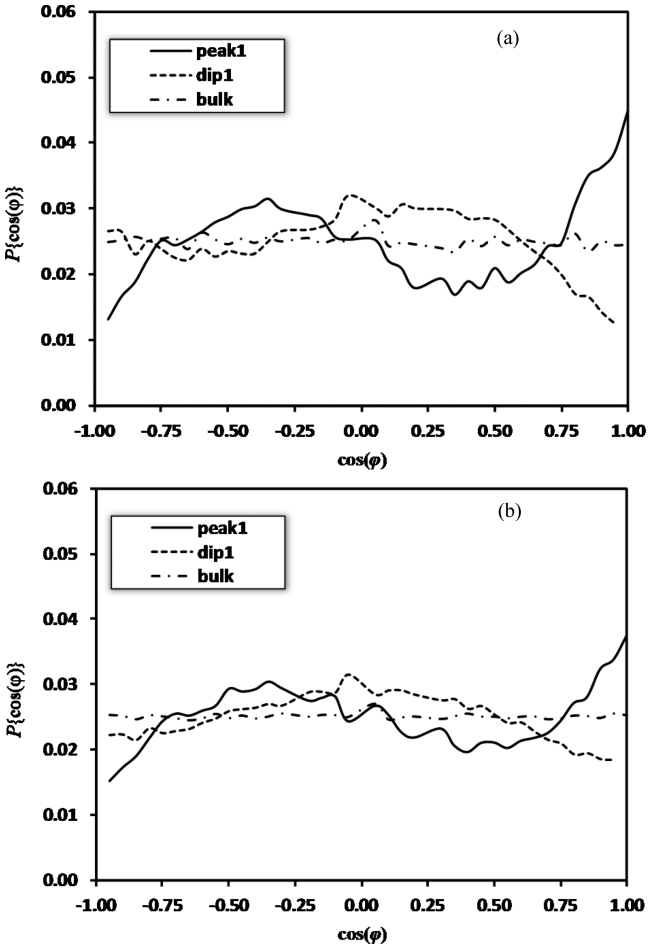

Figure 10. OH bond orientational distributions of water molecules at (a) the normal gas–water interface and (b) the DGL–water interface. Peak 1, dip 1, and bulk are defined in Figure 2.

the solid surface. When the number of gas molecules is less than two layers (across the whole surface), they tend to form cylindrical gas domains. When the number of gas molecules is sufficient to form two layers or more, there only DGLs are formed. The height of the dense gas layer increases with increasing number of nitrogen molecules to maintain the same density in the gas layer.

3.2. Stability of DGL. Even though a DGL may explain the observed attraction of an AFM tip with nanobubbles and gas layer, it is yet to be shown that such a dense layer is stable. To investigate the stability of DGL, we constructed two simulations with different initial densities of the dense nitrogen layer while applying a normal pressure of 1 atm. If there is a stable DGL, the two simulations should end up with same density at equilibrium. If not, the two simulation systems may diverge from one another.

The first simulation started with a grid of nitrogen gas molecules (N = 2250, 6 × 6 × 8 nm) on top of two layers of graphite with water molecules (N = 7754) filling the remainder of the simulation box of 6.9 × 6.6 × 14.0 nm. The initial nitrogen density was around 7.8 nm^{-3} and was referred to as the "compressing" case. The second simulation was identical except the initial grid of nitrogen molecules being more compact so the initial nitrogen density was 14 nm^{-3} and was referred to as the "expanding" case. Both simulations were performed in the NPT ensemble (300 K and 1 atm) to obtain equilibrium density profiles with a running time of 12 ns.

As shown in Figure 7, for the expanding case, the nitrogen density decreased with running time due to the length of nitrogen slab expanding as shown in Figure 8a. After 9 ns running time, the density leveled off at 9.0 ± 0.17 nm^{-3}. For the lower initial nitrogen density ("compressing" case), the bulk nitrogen density increased with running time as shown in Figure 8b. After 9 ns running time, the density leveled off at 8.9 ± 0.15 nm^{-3}, meaning that the equilibrium density was in agreement with the "expanding" case within uncertainty.

In general, due to the significant difference of gas solubility in different solvents, the excess gas molecules will be absorbed by solid particles to form various nanoscopic gas domains. However, we also need to evaluate whether this DGL between water and graphite surface is feasible from the amount of gas available in the solvent exchange system used in AFM experiments.[23] From experimental observations, the height of nanoscopic domains generally ranged from 10 to 100 nm.[10,53] From the experiments using the ethanol–water exchange method for nanobubble formation, the cell volume was around 1 mL with a surface area of 1 × 10^{-4} m^2. The solubility of nitrogen gas in ethanol and water at 300 K and 1 atm is 149 and 8.9 mg/L, respectively.[54] So the excess gas which is produced by ethanol–water exchange in the cell is around 0.14 mg. Even for a DGL height of 100 nm, we need only 0.0042 mg of nitrogen gas to form the gas layer at the high density observed in the simulations presented in this section (9.0 nm^{-3}). So only a small fraction of the nitrogen liberated by the solvent exchange process is required to form the DGL.

dx.doi.org/10.1021/la403187p | Langmuir 2013, 29, 15266–15274

Table 3. Simulation Results for the Liquid−Vapor, Solid−Liquid, and Solid−Vapor Interfacial Tensions, the Cylindrical Contact Angle (θ_c) (Taken from the Water Side), and Young's Contact Angle (θ_Y) Using Eq 5 for Two Different Gas Pressures

simulation conditions for water-graphite interface	interfacial tensions (mN/m)			contact angle (deg)	
	γ_{lv}	γ_{sl}	γ_{sv}	θ_Y	θ_c
normal gas pressure at 1 atm	61.1 ± 1.5	−1.83 ± 0.03	−0.55 ± 0.01	88.8 ± 1.8	85.1 ± 1.5
dense gas pressure at 500 atm	53.8 ± 1.7	−1.83 ± 0.03	−45.8 ± 0.9	144.7 ± 2.1	141.1 ± 1.7

3.3. Interfacial Properties of DGL−Water Interface. An attraction between an AFM tip and nanobubbles was observed by Peng et al.[23] This is in contrast to the interaction between the tip and the submerged graphite surface without nanobubbles which is repulsive. The lack of a significant EDL repulsive force for gas layer−water interface was posited to be due to the reduction in surface potential of an interfacial nanobubble compared to a surface without nanobubbles. To reveal the interfacial properties of the DGL−water and normal−gas interfaces, two different simulation systems were performed.

To understand the normal gas−water interaction, the initial cubic box of water and nitrogen mixtures with ratio of 889:4 (3 × 3 × 3 nm) was set in the middle of a simulation box 3 × 3 × 9 nm. The simulations were performed in the canonical NVT ensemble at 300 K for 3 ns. The calculated number density of water and nitrogen was 33.1 ± 0.5 and 0.04 ± 0.03 nm^{-3}, respectively. As shown in Figure 9a, the calculated apparent interfacial potential for normal gas−water interface is −68 ± 12 mV, which is more negative than the pure water−vapor interface without nitrogen but is closer to the experimental value at −65 mV.[26,27] As shown in Figure 10a, the OH bond orientation at this interface is almost the same as that in Figure 4.

For the other simulation systems, a high density layer of nitrogen gas was placed between water and graphite. A slab of nitrogen gas molecules (N = 2250, 3 × 3 × 6 nm) was placed on top of the graphite layers at a distance of 0.3 nm. The remainder of the simulation box, 6.9 × 6.6 × 12 nm, was filled with water molecules (N = 8001) at the normal water density. The simulation was performed in the NVT ensemble at 300 K for 3 ns. After 2 ns running time, the dense gas layer (DGL) formed between graphite and water. Then, the electrical field and potential profile were calculated for this DGL−water interface and is shown in Figure 9b. The calculated interfacial potential is only −17.5 ± 5 mV, which is much closer to 0 than the value for the normal gas−water interface. As shown in Figure 10b, the orientation profile of the OH bond for the out layer at peak 1 is pointed to the interface normal and away from the water. However, both the orientational distribution profiles (Figure 10) and the electrical field profiles for the DGL−water interface are different from those profiles for normal gas−water interface. This change in interface structure, from normal (1 atm) pressure to high pressure of DGL, results in the large change in surface potential.

3.4. Contact Angle of Cylindrical Gas Domain at Water−Graphite Interface. In addition to the issue of attractive force between the AFM tip and the gas layer, there is the issue of the large contact angles of nanobubbles (from the water side). This has been linked by some researchers to line tension.[10,11,14,53] However, we have indicated that line tension has limited effect on change of contact angle of nanodroplets.[38] We evaluated the contact angle for cylindrical gas domains in the simulations by the method described in section 2.3. We obtained the value of 141.1 ± 1.7° as measured from water side for most cases. This is significantly larger than the contact angle of 85.1 ± 1.5° for water droplet at ambient pressure, as shown in Table 3, but is much closer to the reported nanobubble contact angle values (∼150°) from AFM experiments.[22,50,55,56]

To further investigate the reason for the large contact angles for cylindrical gas domains, we implemented the method for calculating the components of interfacial tension as described in section 2.4. As expressed by Young's equation, the contact angle, θ_Y, made by a macroscopic droplet of a liquid on a smooth solid surface is determined by a balance among the interfacial tensions of the solid-vapor, γ_{sv}, liquid-vapor, γ_{lv}, and solid-liquid, γ_{sl}, interfaces.[57] It is described by

$$\cos(\theta_Y) = \frac{\gamma_{sv} - \gamma_{sl}}{\gamma_{lv}} \quad (5)$$

In the previous research,[38] it has been shown that the contact angles, θ_c, from the cylindrical drops and Young's angle, θ_Y, based on eq 5 agree very well over the range of surface strengths for LJ fluid system. As shown in Table 3, the vapor−liquid interfacial tension is similar to values previously reported for SPC/E water from both MC and MD simulations.[45,58,59] For the water−graphite interfaces, the calculated Young's angle (88.8 ± 1.8°) is close to the "measured" contact angle by cylindrical water droplet on the graphite surface. As for dense gas domain, there is the significant increase in interfacial tension value of graphite−dense gas layer and considerable decrease in interfacial tension of water−dense gas layer. These factors increased the calculated Young's angle up to 144.7 ± 2.1°, which is in good agreement with the value obtained from the cylindrical gas domain as discussed at the beginning of this section.

4. CONCLUSIONS

The molecular simulation work shows that a dense gas layer with a density of 9 nm^{-3} is formed on the water−graphite interface when equilibrated with a normal pressure of 1 atm and temperature of 300 K. By varying the number of gas molecules in the system, we observed several types of dense gas domains, namely, aggregates, cylindrical gas domains, and DGL. Spherical gas domains formed during the simulation but were unstable and always reverted to another type of gas domain. Furthermore, the calculated surface potential of the DGL−water interface, −17.5 mV, is significantly closer to 0 than the surface potential, −65 mV, of normal gas bubble−water interface. The change in surface potential has come from a slight change in the structure of water molecules at the DGL−water interface compared with the normal gas−water interface. This supports our hypothesis from our previous experimental work that the change in surface potential causes the switch from repulsion to attraction for an AFM tip when the graphite surface is covered by a gas layer. In addition, for the cylindrical gas domain, the evaluated contact angle (141°) is far greater than the value of 85° observed for water on graphite at ambient conditions and close to the experimentally measured contact

dx.doi.org/10.1021/la403187p | Langmuir 2013, 29, 15266−15274

angle of nanobubbles (150°). This simulated contact angle was verified by calculating the contact angle with Young's equation using the interfacial tension components which gave the same result within uncertainty (144°). Together, the contact angle and surface potential support the existence of a high density gas layer between water and graphite surface.

AUTHOR INFORMATION

Corresponding Author

*E-mail anh.nguyen@eng.uq.edu.au; Fax +61 7 3365 4199 (A.V.N.).

Notes

The authors declare no competing financial interest.

ACKNOWLEDGMENTS

The authors gratefully acknowledge the financial support from the Australian Research Council (Grant DP0985079) and The University of Queensland Postgraduate Scholarship (UQRS). The authors acknowledge the use of facilities at High Performance Computing Unit, The University of Queensland.

REFERENCES

(1) Parker, J. L.; Claesson, P. M.; Attard, P. Bubbles, Cavities, and the Long-Ranged Attraction between Hydrophobic Surfaces. *J. Phys. Chem.* **1994**, *98* (34), 8468−8480.

(2) Hampton, M. A.; Donose, B. C.; Nguyen, A. V. Effect of Alcohol-Water Exchange and Surface Scanning on Nanobubbles and the Attraction between Hydrophobic Surfaces. *J. Colloid Interface Sci.* **2008**, *325* (1), 267−274.

(3) Zhang, X. H.; Maeda, N.; Craig, V. S. J. Physical Properties of Nanobubbles on Hydrophobic Surfaces in Water and Aqueous Solutions. *Langmuir* **2006**, *22* (11), 5025−5035.

(4) Zhang, X. H.; Li, G.; Wu, Z. H.; Zhang, X. D.; Hu, J. Effect of Temperature on the Morphology of Nanobubbles at Mica/Water Interface. *Chin. Phys.* **2005**, *14*, 1774−1778.

(5) Seddon, J. R. T.; Kooij, E. S.; Poelsema, B.; Zandvliet, H. J. W.; Lohse, D. Surface Bubble Nucleation Stability. *Phys. Rev. Lett.* **2011**, *106* (5), 56101.

(6) Yang, S.; Dammer, S. M.; Bremond, N.; Zandvliet, H. J. W.; Kooij, E. S.; Lohse, D. Characterization of Nanobubbles on Hydrophobic Surfaces in Water. *Langmuir* **2007**, *23* (13), 7072−7077.

(7) Yang, S.; Tsai, P.; Kooij, E. S.; Prosperetti, A.; Zandvliet, H. J. W.; Lohse, D. Electrolytically Generated Nanobubbles on Highly Orientated Pyrolytic Graphite Surfaces. *Langmuir* **2009**, *25* (3), 1466−1474.

(8) Zhang, L.; Zhang, Y.; Zhang, X.; Li, Z.; Shen, G.; Ye, M.; Fan, C.; Fang, H.; Hu, J. Electrochemically Controlled Formation and Growth of Hydrogen Nanobubbles. *Langmuir* **2006**, *22* (19), 8109−8113.

(9) Anh, V. N.; Marc, A. H. The Nanobubble Story. In *Encyclopedia of Surface and Colloid Science*, 2nd ed.; Taylor & Francis: New York, 2012; pp 1−15.

(10) Seddon, J. R. T.; Lohse, D. Nanobubbles and Micropancakes: Gaseous Domains on Immersed Substrates. *J. Phys.: Condens. Matter* **2011**, *23*, 133001.

(11) Hampton, M. A.; Nguyen, A. V. Nanobubbles and the Nanobubble Bridging Capillary Force. *Adv. Colloid Interface Sci.* **2010**, *154* (1−2), 30−55.

(12) Karpitschka, S.; Dietrich, E.; Seddon, J. R. T.; Zandvliet, H. J. W.; Lohse, D.; Riegler, H. Nonintrusive Optical Visualization of Surface Nanobubbles. *Phys. Rev. Lett.* **2012**, *109* (6), 066102.

(13) Chan, C. U.; Ohl, C.-D. Total-Internal-Reflection-Fluorescence Microscopy for the Study of Nanobubble Dynamics. *Phys. Rev. Lett.* **2012**, *109* (17), 174501.

(14) Craig, V. S. J. Very Small Bubbles at Surfaces-the Nanobubble Puzzle. *Soft Matter* **2011**, *7* (1), 40−48.

(15) Ducker, W. A. Contact Angle and Stability of Interfacial Nanobubbles. *Langmuir* **2009**, *25* (16), 8907−8910.

(16) Brenner, M. P.; Lohse, D. Dynamic Equilibrium Mechanism for Surface Nanobubble Stabilization. *Phys. Rev. Lett.* **2008**, *101* (21), 214505.

(17) Dammer, S. M.; Lohse, D. Gas Enrichment at Liquid-Wall Interfaces. *Phys. Rev. Lett.* **2006**, *96* (20), 206101.

(18) Zhang, L.; Wang, C.; Tai, R.; Hu, J.; Fang, H. The Morphology and Stability of Nanoscopic Gas States at Water/Solid Interfaces. *ChemPhysChem* **2012**, *13* (8), 2188−2195.

(19) Wang, C.-L.; Zhao-Xia, L.; Jing-Yuan, L.; Peng, X.; Jun, H.; Hai-Ping, F. High Density Gas State at Water/Graphite Interface Studied by Molecular Dynamics Simulation. *Chin. Phys. B* **2008**, *17*, 2646.

(20) Zhang, X.; Chan, D. Y. C.; Wang, D.; Maeda, N. Stability of Interfacial Nanobubbles. *Langmuir* **2013**, *29* (4), 1017−1023.

(21) Weijs, J. H.; Lohse, D. Why Surface Nanobubbles Live for Hours. *Phys. Rev. Lett.* **2013**, *110* (5), 054501.

(22) Seddon, J. R. T.; Lohse, D.; Ducker, W. A.; Craig, V. S. J. A Deliberation on Nanobubbles at Surfaces and in Bulk. *ChemPhysChem* **2012**, *13*, 2179−2187.

(23) Peng, H.; Hampton, M. A.; Nguyen, A. V. Nanobubbles Do Not Sit Alone at the Solid-Liquid Interface. *Langmuir* **2013**, *29* (20), 6123−6130.

(24) Churaev, N.; Derjaguin, B. Inclusion of Structural Forces in the Theory of Stability of Colloids and Films. *J. Colloid Interface Sci.* **1985**, *103* (2), 542−553.

(25) Derjaguin, B. A Theory of the Heterocoagulation, Interaction and Adhesion of Dissimilar Particles in Solutions of Electrolytes. *Discuss. Faraday Soc.* **1954**, *18*, 85−98.

(26) Taran, E.; Hampton, M. A.; Nguyen, A. V.; Attard, P. Anomalous Time Effect on Particle-Bubble Interactions Studied by Atomic Force Microscopy. *Langmuir* **2009**, *25* (5), 2797−2803.

(27) Graciaa, A.; Morel, G.; Saulner, P.; Lachaise, J.; Schechter, R. S. The ζ-Potential of Gas Bubbles. *J. Colloid Interface Sci.* **1995**, *172* (1), 131−136.

(28) Paruchuri, V. K.; Nguyen, A. V.; Miller, J. D. Zeta-Potentials of Self-Assembled Surface Micelles of Ionic Surfactants Adsorbed at Hydrophobic Graphite Surfaces. *Colloids Surf., A* **2004**, *250* (1−3), 519−526.

(29) Bratko, D.; Luzar, A. Attractive Surface Force in the Presence of Dissolved Gas: A Molecular Approach. *Langmuir* **2008**, *24* (4), 1247−1253.

(30) Sendner, C.; Horinek, D.; Bocquet, L.; Netz, R. R. Interfacial Water at Hydrophobic and Hydrophilic Surfaces: Slip, Viscosity, and Diffusion. *Langmuir* **2009**, *25* (18), 10768−10781.

(31) Berendsen, H.; Postma, J.; Van Gunsteren, W.; Hermans, J. Interaction Models for Water in Relation to Protein Hydration. *Intermol. Forces* **1981**, 331−342.

(32) Taylor, R. S.; Dang, L. X.; Garrett, B. C. Molecular Dynamics Simulations of the Liquid/Vapor Interface of SPC/E Water. *J. Phys. Chem.* **1996**, *100* (28), 11720−11725.

(33) Jaffe, R.; Gonnet, P.; Werder, T.; Walther, J.; Koumoutsakos, P. Water−Carbon Interactions 2: Calibration of Potentials Using Contact Angle Data for Different Interaction Models. *Mol. Simul.* **2004**, *30* (4), 205−216.

(34) Werder, T.; Walther, J.; Jaffe, R.; Halicioglu, T.; Koumoutsakos, P. On the Water-Carbon Interaction for Use in Molecular Dynamics Simulations of Graphite and Carbon Nanotubes. *J. Phys. Chem. B* **2003**, *107* (6), 1345−1352.

(35) Werder, T.; Walther, J.; Jaffe, R.; Halicioglu, T.; Noca, F.; Koumoutsakos, P. Molecular Dynamics Simulation of Contact Angles of Water Droplets in Carbon Nanotubes. *Nano Lett.* **2001**, *1* (12), 697−702.

(36) Van Der Spoel, D.; Lindahl, E.; Hess, B.; Groenhof, G.; Mark, A. E.; Berendsen, H. J. C. GROMACS: Fast, Flexible, and Free. *J. Comput. Chem.* **2005**, *26* (16), 1701−1718.

(37) Gonzalez, M. A.; Abascal, J. L. F. The Shear Viscosity of Rigid Water Models. *J. Chem. Phys.* **2010**, *132* (9), 096101.

(38) Peng, H.; Nguyen, A.; Birkett, G. The Impact of Line Tension on the Contact Angle of Nanodroplets. *Mol. Simul.* **2013**, In press.
(39) Peng, H.; Nguyen, A. V.; Birkett, G. R. Determination of Contact Angle by Molecular Simulation Using Number and Atomic Density Contours. *Mol. Simul.* **2012**, *38* (12), 945−952.
(40) Steele, W. A. The Interaction of Rare Gas Atoms with Graphitized Carbon Black. *J. Phys. Chem.* **1978**, *82* (7), 817−821.
(41) Steele, W. A. The Physical Interaction of Gases with Crystalline Solids: I. Gas-Solid Energies and Properties of Isolated Adsorbed Atoms. *Surf. Sci.* **1973**, *36* (1), 317−352.
(42) Peng, H.; Nguyen, A.; Birkett, G. A Weighted Test-Area Method for Calculating Surface Tension. *Mol. Simul.* **2013**, *39* (2), 129−136.
(43) Wick, C. D.; Dang, L. X.; Jungwirth, P. Simulated Surface Potentials at the Vapor-Water Interface for the KCl Aqueous Electrolyte Solution. *J. Chem. Phys.* **2006**, *125* (2), 024706.
(44) Wilson, M. A.; Pohorille, A.; Pratt, L. R. Surface Potential of the Water Liquid–Vapor Interface. *J. Chem. Phys.* **1988**, *88* (5), 3281−3285.
(45) dos Santos, D. J. V. A.; Müller-Plathe, F.; Weiss, V. C. Consistency of Ion Adsorption and Excess Surface Tension in Molecular Dynamics Simulations of Aqueous Salt Solutions. *J. Phys. Chem. C* **2008**, *112* (49), 19431−19442.
(46) Elmahdy, A. M.; Mirnezami, M.; Finch, J. A. Zeta Potential of Air Bubbles in Presence of Frothers. *Int. J. Miner. Process.* **2008**, *89*, 40−43.
(47) Fan, X.; Zhang, Z.; Li, G.; Rowson, N. A. Attachment of Solid Particles to Air Bubbles in Surfactant-Free Aqueous Solutions. *Chem. Eng. Sci.* **2004**, *59* (13), 2639−2645.
(48) Janecek, J.; Netz, R. R. Interfacial Water at Hydrophobic and Hydrophilic Surfaces:Depletion versus Adsorption. *Langmuir* **2007**, *23* (16), 8417−8429.
(49) Lu, Y.-H.; Yang, C.-W.; Hwang, I.-S. Molecular Layer of Gaslike Domains at a Hydrophobic-Water Interface Observed by Frequency-Modulation Atomic Force Microscopy. *Langmuir* **2012**, *28* (35), 12691−12695.
(50) Zhang, L.; Zhang, X.; Fan, C.; Zhang, Y.; Hu, J. Nanoscale Multiple Gaseous Layers on a Hydrophobic Surface. *Langmuir* **2009**, *25* (16), 8860−8864.
(51) Zhang, X. H.; Zhang, X.; Sun, J.; Zhang, Z.; Li, G.; Fang, H.; Xiao, X.; Zeng, X.; Hu, J. Detection of Novel Gaseous States at the Highly Oriented Pyrolytic Graphite-Water Interface. *Langmuir* **2006**, *23* (4), 1778−1783.
(52) Linstrom, P.; Mallard, W. *NIST Chemistry WebBook*; NIST Standard Reference Database Number 69; National Institute of Standards and Technology: Gaithersburg, MD 20899 (http://webbook.nist.gov).
(53) Zhang, L.; Zhang, X.; Zhang, Y.; Hu, J.; Fang, H. The Length Scales for Stable Gas Nanobubbles at Liquid/Solid Surfaces. *Soft Matter* **2011**, *6* (18), 4515−4519.
(54) Tochigi, K.; Kojima, K. Prediction of Non-polar Gas Solubilities in Water, Alcohols and Aqueous Alcohol Solutions by the Modified asog Method. *Fluid Phase Equilib.* **1982**, *8* (3), 221−232.
(55) Song, B.; Walczyk, W.; Schönherr, H. Contact Angles of Surface Nanobubbles on Mixed Self-Assembled Monolayers with Systematically Varied Macroscopic Wettability by Atomic Force Microscopy. *Langmuir* **2011**, *27*, 8223−8232.
(56) Borkent, B. M.; de Beer, S.; Mugele, F.; Lohse, D. On the Shape of Surface Nanobubbles. *Langmuir* **2009**, *26* (1), 260−268.
(57) Young, T. An Essay on the Cohesion of Fluids. *Philos. Trans. R. Soc. London* **1805**, *95*, 65−87.
(58) Vega, C.; Miguel, E. d. Surface Tension of the Most Popular Models of Water by Using the Test-Area Simulation Method. *J. Chem. Phys.* **2007**, *126* (15), 154707.
(59) Chen, F.; Smith, P. E. Simulated Surface Tensions of Common Water Models. *J. Chem. Phys.* **2007**, *126* (22), 221101.
(60) The shapes are defined using the density profiles (similar to the Gibbs dividing surface). We successfully applied this approach in simulating contact angles in refs 38 and 39. Here we define the structure of various domains based on the density distribution cross the surface (*x*- and *y*-axes) and height density profile (*z*-axis). For aggregates, the gas molecules randomly distribute at the solid surface, and there is only one peak at the height density profile. For spherical drop, most of the gas molecules nucleate at the solid surface and do not spread across the surface. The height of drop is higher than the corresponding cylindrical shape. For cylindrical drop, most of the gas molecules also nucleate at the solid surface but spread along one axis (such as *y*-axis) to form a cylindrical shape. The height density profile is similar to the line of Nitrogen_0.8 ns in Figure 8a. For DGL, the gas molecules spread cross the whole surface to form a layer structure. The height density profile is similar as the line of Nitrogen_5.6 ns in Figure 8a.